Transport collision integrals for C(⁵S)-H(²S), C(¹S)-H(²S), C(¹D)-H(²S), and C(³P)-H(²S) interactions ⊘

Zhenlu Hou (后振鲁) (iD) ; Zhi Qin (秦智) ✉ (iD) ; Linhua Liu (刘林华) (iD)

Check for updates

View Online   Export Citation   CrossMark

Articles You May Be Interested In

Scattering cross sections and collision integrals for N(⁴S)–N⁺(³P) and N(⁴S)–N⁺(¹D) interactions

Physics of Fluids (August 2023)

Collision integrals for N(⁴S)–N(⁴S), N(⁴S)–N(²D), and N(⁴S)–N(²P) interactions

Physics of Fluids (February 2023)

Energy natural orbitals

J. Chem. Phys. (March 2021)

Transport collision integrals for C(⁵S)-H(²S), C(¹S)-H(²S), C(¹D)-H(²S), and C(³P)-H(²S) interactions

View Online   Export Citation   CrossMark

Zhenlu Hou (后振鲁),[1,2] [ID] Zhi Qin (秦智),[1,2,a] [ID] and Linhua Liu (刘林华)[1,2,3,b] [ID]

AFFILIATIONS

[1]Optics and Thermal Radiation Research Center, Institute of Frontier and Interdisciplinary Science, Shandong University, Qingdao 266237, People's Republic of China
[2]School of Energy and Power Engineering, Shandong University, Jinan 250061, People's Republic of China
[3]School of Energy Science and Engineering, Harbin Institute of Technology, Harbin 150001, People's Republic of China

[a]Author to whom correspondence should be addressed: z.qin@sdu.edu.cn
[b]liulinhua@sdu.edu.cn

ABSTRACT

Transport collision integrals of interacting atoms or ions are essential in modeling transport properties of high-temperature gases and plasmas. Here, we obtained the potential energy curves (PECs) of CH using the state-of-the-art *ab initio* methods. The PECs were also extrapolated to investigate the transport collision integrals for C(³P)-H(²S), C(⁵S)-H(²S), C(¹S)-H(²S), and C(¹D)-H(²S) interactions, in which the interactions between the excited C(⁵S), C(¹S), and C(¹D) atoms and the ground H(²S) atoms were calculated for the first time. The resulting transport collision integrals were fitted to simple functional forms for ease of use in plasma modeling. Our transport collision integrals can provide data references for computing transport properties of high-temperature plasmas involving C and H atoms.

I. INTRODUCTION

The methylidyne radical, CH, is formed in various astrophysical environments.[1] This radical was first detected in the laboratory as early as 1918.[2,3] The existence of the CH radical in the interstellar space was first identified by Swings and Rosenfeld[4] in 1937. Subsequently, CH has been detected in the sun,[5–8] stellar atmospheres,[9,10] diffuse interstellar bands,[11–13] comets,[14] interstellar medium,[15,16] dust clouds,[17–19] the diffuse interstellar clouds,[20] dark clouds,[21,22] stars,[23] and extragalactic galaxies.[24]

The CH plasmas have also attracted great attention in other applications. For example, the methane-air plasma is a mixture consisting of e/C/H/N/O.[25] The CH plasma is closely linked with the critical fusion reactor design issue of tritium codeposition in tokamaks with carbon as the wall material.[26] The CH plasma can provide an environment in modeling parametric instabilities excited by a single, intense, wavelength-sized laser speckle.[27] The CH plasma was chosen as the standard ablator material for ignition capsules in National Ignition Facility.[28] Moreover, the CH plasma was widely used in laser–plasma experiments because it is easy to deal with and to form into special targets.[29–31] Hence, investigating various properties of plasmas including C and H is particularly important in applications mentioned above, and the transport properties of plasmas, including viscosity, thermal conductivity, electrical conductivity, and so on, are essential for the study of plasma fluid dynamics. Solving the mass, momentum, and energy equations, together with electromagnetic field equations, depends on suitable transport properties.[25,32,33] The transport properties can be calculated using the well-known Chapman–Enskog theory based on transport collision integrals. For example, the viscosity in the first-order approximation is given by[34]

$$\eta = \frac{5}{16} \frac{(\pi m k_B T)^{1/2}}{\pi \sigma^2 \Omega^{(2,2)*}}, \tag{1}$$

where k_B is the Boltzmann constant, m is the mass of the molecule, σ is the collision diameter, $\sigma^2 \Omega^{(2,2)*}$ is the reduced transport collision integral, and T is the temperature. Therefore, the accuracy of transport properties strongly relies on the reliability of transport collision integrals.[35,36]

In the last few decades, great attention has been dedicated to the calculation of transport collision integrals of high-temperature species.[37–39] The high-temperature environment can trigger different types of interactions, including neutral–neutral,[38,40–42] neutral–ion,[37,41–43] electron–neutral,[41,42] and ion–ion[44,45] interactions. The high-temperature environment can also contribute to the formation of

excited-state neutrals and ions. Determining the transport collision integrals for these interactions relies on the underlying potential energy curves (PECs).

There are currently three options for obtaining potential energies in the calculation of transport collision integrals: the analytical potential functions determined from several spectroscopic parameters, the *ab initio* potential energy points, and the analytical functions fitted from *ab initio* points. Frequently used analytical potential energy functions to calculate the transport collision integrals, such as Lennard–Jones (LJ),[46–51] m-6-8,[52,53] Hulburt–Hirschfelder (HH),[52,54–57] Murrell–Sorbie (MS),[58] and modified morse (MM)[59] potentials, rely on the experimental spectroscopic data and can produce accurate potential wells of PECs. However, there are questionable in the dissociated asymptotic and short-range regions, leading to uncertainty in the resulting transport collision integrals. In addition, excited (in particular repulsive) states are thought to play an equally vital role in determining the transport collision integrals.[45] Also, using a simple exponential function to represent the repulsive curves is not appropriate for the calculation of reliable transport collision integrals in a wide temperature range.[40] The problems mentioned above can be alleviated using high-quality PECs. Therefore, precise PECs are needed to obtain reliable transport collision integrals and to effectively predict transport properties.

With the development of *ab initio* methods,[60–63] the computational accuracy of PECs has improved significantly. *Ab initio* potential energy data can be accepted as a baseline when experimental spectroscopic data are not available. Aziz *et al.*[64] obtained the precise transport properties and virial coefficients of helium based on the state-of-the-art *ab initio* PECs in 1995. More recently, Buchowiecki and Szabó[45] calculated the transport collision integrals for the H–N$^+$, N–H$^+$, N^{2+}–H, and N$^+$–H$^+$ interactions in the temperature range of 1000–60 000 K using the interpolation and extrapolation of *ab initio* potential energy points, simultaneously considering excited (in particular repulsive) states. The transport cross sections and integrated cross sections are also reported by Buchowiecki[65] for interactions of hydrogen and nitrogen atoms and ions (in the ground and excited states) using extrapolated *ab initio* PECs. Ding *et al.*[38] calculated transport collision integrals for N(^{4}S)–N(^{4}S), N(^{4}S)–N(^{2}D), and N(^{4}S)–N(^{2}P) interactions based on the combined-hyperbolic-inverse-power-representation (CHIPR)[66,67] PECs obtained from fitting *ab initio* points. The CHIPR method is detailed in previous publications[68–76] and can obtain reasonable behaviors for *ab initio* potential energy points. Therefore, the CHIPR method needs sufficient *ab initio* potential points covering theoretically reasonable internuclear distances for accurately calculating the cross sections and transport collision integrals. The CHIPR method can give nearly the same transport collision integrals as those from the interpolation and extrapolation of *ab initio* potential energy points, but this method may cost huge time on fitting PECs for all the electronic states. Therefore, using the interpolation and extrapolation of *ab initio* potential energy points is a good choice for highly accurate calculations of transport collision integrals.[45]

As early as 2006, Sourd *et al.*[25] determined the transport properties of e/C/H/N/O mixtures in the temperature range of 9000–20 000 K, including C(^{3}P)–H(^{2}S) interaction. Sanon and Baronnet[77] calculated the transport collision integrals for the thermal plasma composed of Ar/C/H/O/N in the temperature range from 1000 to 15 000 K. More recently, transport properties for neutral C, H, N, O,

and Si-containing species and mixtures were studied by Bellas Chatzigeorgis *et al.*,[35] considering the CH molecule. However, previous studies only focused on the interaction between the ground C(^{3}P) and H(^{2}S) atoms and did not provide the collision integral data for CH. The interactions between the atomic ground and excited states are also of paramount importance at high temperatures, which mainly results from the fact that the importance of the excited atoms depends on their numbers, which increase with increasing temperature.[45]

Taking above into consideration, we, therefore, revisit the transport collision integrals for C(^{3}P)–H(^{2}S) interaction using the state-of-the-art *ab initio* PECs, as well as the interactions between the excited C(^{5}S), C(^{1}S), and C(^{1}D) atoms and the ground H(^{2}S) atoms, which are considered for the first time. Section II provides the methods for computing the PECs and transport collision integrals. Section III discusses the results of the PECs and transport collision integrals. Finally, a conclusion is drawn in Sec. IV.

II. THEORY AND METHODS
A. *Ab initio* calculations of potential energy curves

In this work, PECs of ten electronic states, including the A $^2\Delta$, E $^2\Pi$, X $^2\Pi$, C $^2\Sigma^+$, D $^2\Sigma^+$, B $^2\Sigma^-$, c $^4\Sigma^-$, b $^4\Pi$, a $^4\Sigma^-$, and d $^6\Sigma^-$ states, correlating to the first four dissociation channels of the CH radical were calculated with the MOLPRO 2015 quantum chemistry package.[78,79] The PECs are obtained using the state-averaged complete active space self-consistent field (SA-CASSCF) approach,[80,81] followed by internally contracted multireference configuration interaction with the Davidson correction (icMRCI+Q),[82–85] which is widely used to study PECs of diatomic molecules.[38,86–90] The calculation is performed in the largest Abelian subgroup (C_{2v}) because MOLPRO cannot deal with the symmetry of the non-Abelian ($C_{\infty v}$) symmetry. The irreducible representation of the C_{2v} point group is (A_1, B_1, B_2, A_2), and its corresponding relationship to $C_{\infty v}$ point group can be described as follows: $\Sigma^+ \rightarrow A_1$, $\Sigma^- \rightarrow A_2$, $\Pi \rightarrow (B_1, B_2)$, and $\Delta \rightarrow (A_1, A_2)$. The aug-cc-pwCV5Z-DK basis set[91] is selected for the C atom, and the aug-cc-pV5Z basis set is selected for the H atom. The PECs of the quartet and sextet electronic states were computed at the internuclear distances from 0.4 to 9.5 Å with step sizes of 0.05 Å for 0.4–1.2 Å, 0.02 Å for 1.2–2 Å, 0.05 Å for 2–4 Å, 0.1 Å for 4–5 Å, and 0.5 Å for 5–9.5 Å, and those for the doublet electronic states were computed at the internuclear distances from 0.44 to 10 Å with step sizes of 0.02 Å for 0.44–2 Å, 0.05 Å for 2–4 Å, 0.1 Å for 4–5 Å, and 0.5 Å for 5–10 Å.

For the calculation of transport collision integrals, *ab initio* PECs are needed to be extrapolated over the short and long ranges of internuclear distance R. In this work, the PECs are extrapolated by the following function for the short-range region:

$$V(R) = A \exp(-BR) + C, \tag{2}$$

where A, B, and C are fitting parameters and are determined from *ab initio* energies calculated using at least three different *ab initio* potential energy values for R in the short-range region, which are usually potential energy points corresponding to three minimum internuclear distances. The cubic spline was used to interpolate the *ab initio* points. To ensure continuous and smooth PECs, the long-range region can be extrapolated by the following function:

$$V(R) = -\frac{C_5}{R^5} - \frac{C_6}{R^6} + V(R \rightarrow \infty), \tag{3}$$

TABLE I. Statistical weights of the electronic states of CH.

State	w_i	State	w_i
$^2\Sigma^+$	2/30	$^4\Sigma^+$	4/30
$^2\Sigma^-$	2/30	$^4\Pi$	8/30
$^2\Delta$	4/30	$^6\Sigma^-$	6/30

TABLE II. Electronic states of CH and their corresponding dissociation limits.

Dissociation limit	Molecular electronic states
$C(^5S)$–$H(^2S)$	$c\ ^4\Sigma^-$, $d\ ^6\Sigma^-$
$C(^1S)$–$H(^2S)$	$D\ ^2\Sigma^+$
$C(^1D)$–$H(^2S)$	$C\ ^2\Sigma^+$, $E\ ^2\Pi$, $A\ ^2\Delta$
$C(^3P)$–$H(^2S)$	$X\ ^2\Pi$, $B\ ^2\Sigma^-$, $b\ ^4\Pi$, $a\ ^4\Sigma^-$

where C_5 and C_6 are state-dependent coefficients, which were estimated by fitting *ab initio* points in this work.

We should note that *ab initio* potential energy points calculated in this work have covered a wide range of internuclear distances. The maximum potential energies at the minimum internuclear distance for all the electronic states considered here are more than 1.5 Hartree above their dissociation limits, which will remarkably reduce the error of transport collision integrals due to the extrapolation of the *ab initio* potential energy points and enable accurate calculation of transport collision integrals. About the extrapolation of Eq. (1), previous works[92,93] compared the potential energies determined from different *ab initio* levels of theory with those fitted by Eq. (1). The results show that Eq. (1) is seen to be an excellent function for fitting the potential energies with the root mean square (RMS) errors of the order of 0.1 mE_h for the calculated potential energies using a variety of *ab initio* methods, including the restricted Hartree–Fock (RHF) SCF, the second-order Møller–Plesset perturbation theory (MP2), and CASSCF/internally contracted CI method. The error of the potential energies obtained from the complete basis set (CBS) model theory
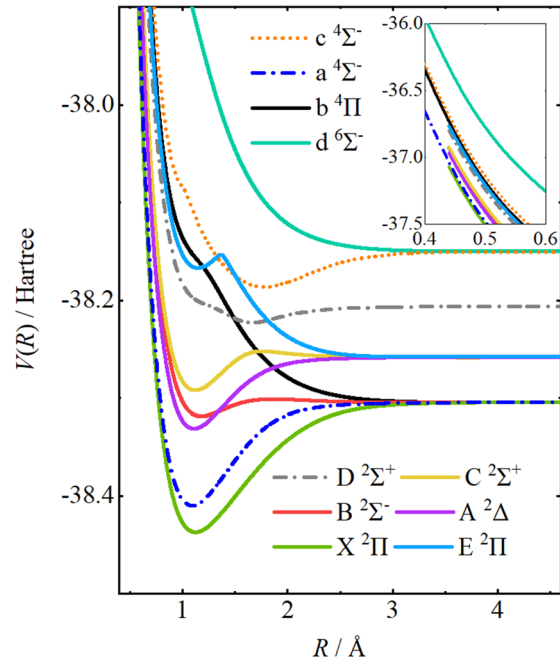

FIG. 1. Potential energy curves of CH calculated by the icMRCI method with the aug-cc-pwCV5Z-DK basis set for the C atom and the aug-cc-pV5Z basis set for the H atom.

proposed by Petersson et al.[94,95] reaches 0.28 mE_h. These results verified the validity of Eq. (1). For the extrapolation of Eq. (2), previous studies[96,97] show that the long-range interaction potential between two neutral atoms of the separation R can be expressed as a power series in $1/R$ and Eq. (2) is just from Eq. (1) of the paper from Yan et al.[97] The first two terms in Eq. (1) of the paper from Yan et al.[97] are thought to be the most important. Of course, C_5 and C_6 can be obtained using the theories of long-range interaction potentials.[98] In this work, C_5 and C_6 were estimated by fitting *ab initio* potential energy points while keeping the dissociation limits fixed, just as done in previous studies.[99,100]
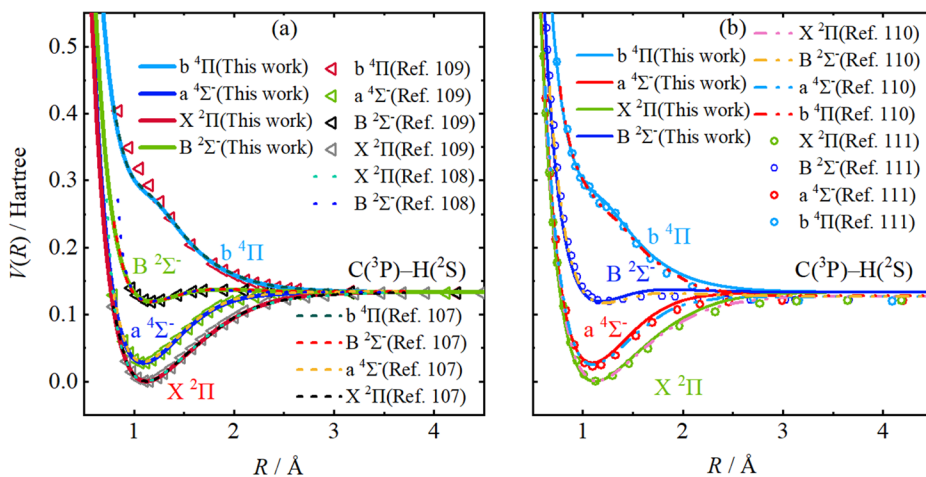

FIG. 2. Comparison of the PECs for CH correlating to the $C(^3P)$–$H(^2S)$ dissociation limit relative to the lowest point of the ground state with those from (a) Refs. 107–109, (b) Refs. 110 and 111.
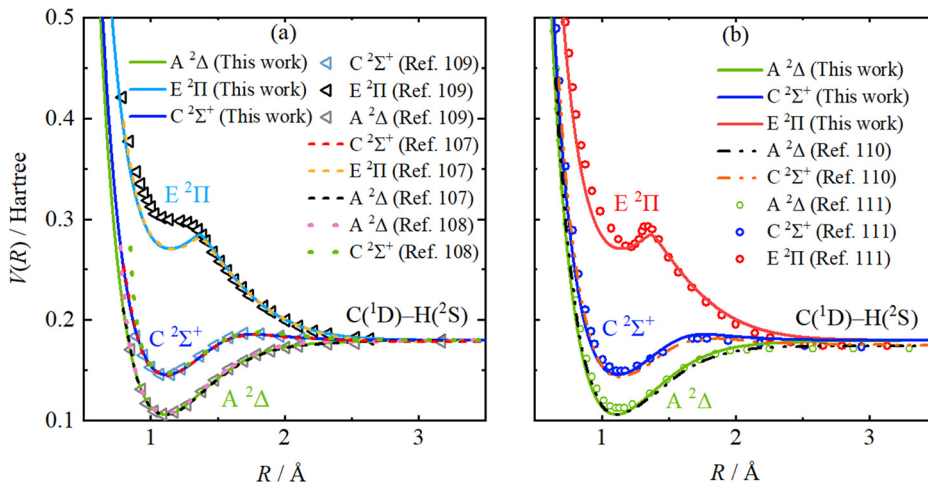
FIG. 3. Comparison of the PECs for CH dissociating to the C(^{1}D)–H(^{2}S) asymptote relative to the lowest point of the ground state with those from (a) Refs. 107–109, (b) Refs. 110 and 111.

Such treatment can ensure a smooth transition between *ab initio* potential points and the extrapolated potential energies.

B. Calculation of the transport collision integrals

The deflection angle of scattering atoms interacting with potential energy $V(R)$ is expressed as follows:[101]

$$\chi(b,\gamma) = \pi - 2b \int_{r_c}^{\infty} dR / \left[R^2 \sqrt{1 - b^2/R^2 - V(R)/(k_B T \gamma^2)} \right], \quad (4)$$

where b is the impact parameter, r_c is the distance of the closest approach, R is the internuclear distance, $\gamma^2 = \mu g^2/(2k_B T)$, μ is the reduced mass, and g is the relative velocity. Given the deflection angle χ for an impact parameter b, the collision cross section can be obtained by

$$Q^l(\gamma) = 2\pi \int_0^{\infty} \left[1 - \cos^l \chi(b,\gamma) \right] b \, db. \quad (5)$$

Reduced transport collision integral is the ratio of the transport collision integral using a particular energy model divided by the rigid sphere model value,[34,40,45,51,102,103]

$$\sigma^2 \Omega^{(l,s)*} = \frac{2}{\pi(s+1)! \left[1 - \frac{1 + (-1)^l}{2(1+l)} \right]} \int_0^{\infty} e^{-\gamma^2} \gamma^{2s+3} Q^l(\gamma) d\gamma, \quad (6)$$

where (l,s) is the order of the transport collision integrals. If two particles interact according to more than one PEC, then the transport collision integral is defined as the weighted average,

FIG. 4. Comparison of the PECs for CH relating to the C(^{1}S)–H(^{2}S) dissociation limit relative to the lowest point of the ground state with those from Refs. 109 and 111.
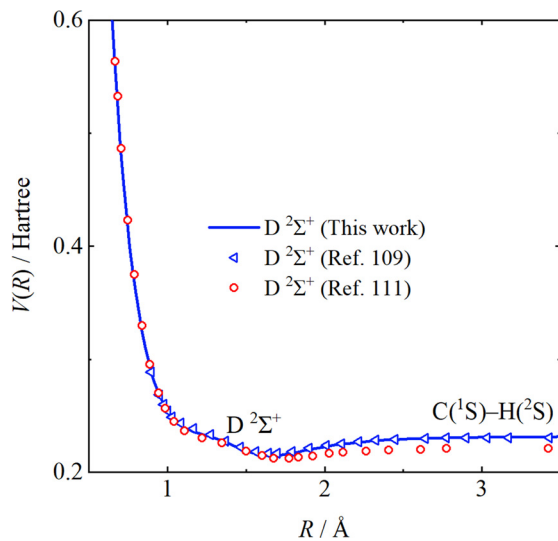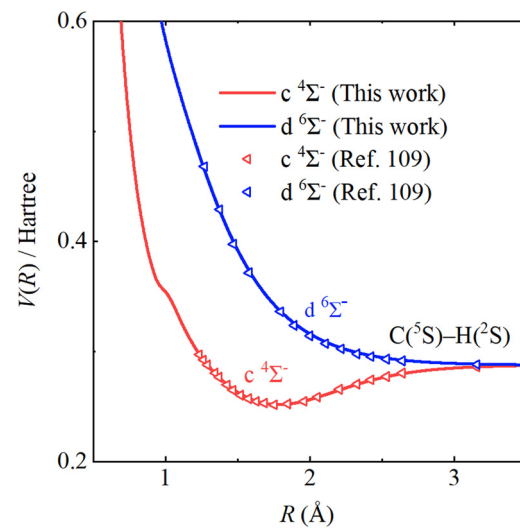

FIG. 5. Comparison of the PECs for CH for the C(^{5}S)–H(^{2}S) dissociation limit relative to the lowest point of the ground state with those from Ref. 109.

$$\sigma^2 \Omega_{av}^{(l,s)*} = \frac{\sum_i w_i \sigma^2 \Omega_i^{(l,s)*}}{\sum_i w_i}, \qquad (7)$$

where w_i are the statistical weights according to molecular term symbols[104–106] and listed in Table I. $\sigma^2 \Omega_i^{(l,s)*}$ is the reduced transport collision integral associated with every dissociation limit at the ith electronic state.

III. RESULTS AND DISCUSSION

Ten electronic states of CH and their corresponding dissociation limits are shown in Table II. Figure 1 shows the computed PECs of these ten electronic states. At the C(^{3}P)–H(^{2}S) dissociation limit, there exist four electronic states, including X $^2\Pi$, B $^2\Sigma^-$, b $^4\Pi$, and a $^4\Sigma^-$ states. It is worth noting that the b $^4\Pi$ state is repulsive, while X $^2\Pi$, B $^2\Sigma^-$, and a $^4\Sigma^-$ states have potential wells of varying depths. At the C

(^{1}D)–H(^{2}S) dissociation limit, both C $^2\Sigma^+$ and A $^2\Delta$ states have potential wells, whereas the E $^2\Pi$ state has a potential well and a potential barrier above its dissociation limit. There only has one electronic state at the C(^{1}S)–H(^{2}S) dissociation limit, namely, the D $^2\Sigma^+$ state, which has a shallow potential well. At the C(^{5}S)–H(^{2}S) dissociation limit, the c $^4\Sigma^-$ state has a potential well and the d $^6\Sigma^-$ state is repulsive.

In order to verify the reliability of our *ab initio* data, comparisons between our PECs correlating to the first four dissociation channels of the CH radical and those computed by other researchers are shown in Figs. 2–5. Solid lines represent our PECs calculated using the icMRCI method with the aug-cc-pwCV5Z-DK basis set for the C atom and aug-cc-pV5Z basis set for the H atom. Dashed lines represent the PECs calculated by Abdallah *et al.*[107] using the multi-reference configuration interaction (MRCI) method with the aug-cc-pVQZ basis set. Short dotted lines stand for the PECs computed by Billoux *et al.*[108] using the Rydberg–Klein–Rees (RKR) inversion method. Triangular symbols are the PECs calculated by Kalemos
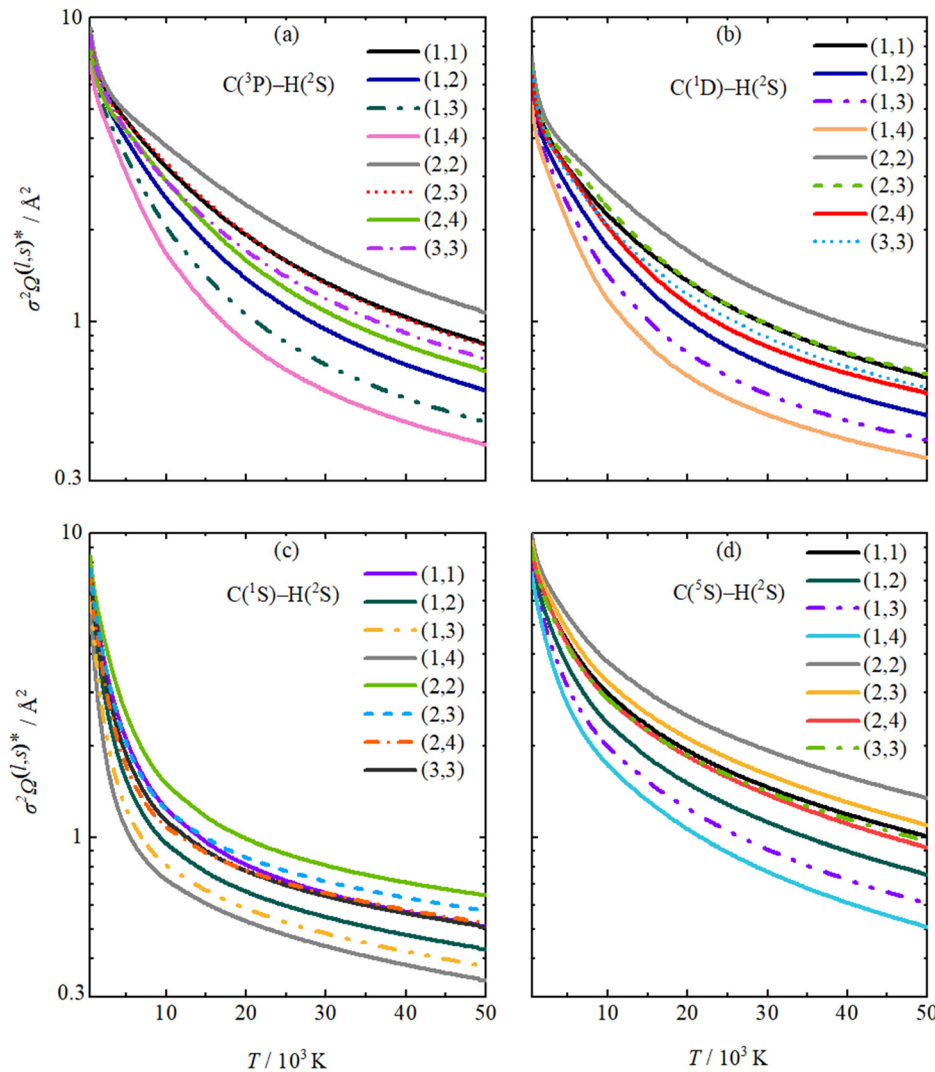

FIG. 6. Transport collision integrals of (a) C(^{3}P)–H(^{2}S), (b) C(^{1}D)–H(^{2}S), (c) C(^{1}S)–H(^{2}S), and (d) C(^{5}S)–H(^{2}S) interactions.

et al.[109] using the MRCI method with the cc-pVQZ basis set for the H atom and cc-pV6Z basis set for the C atom. Double dotted lines represent the PECs computed by Song *et al.*[110] using spin–orbit multiconfiguration quasi-degenerate perturbation theory (SO-MCQDPT). Circular symbols are the PECs calculated by Chakrabarti *et al.*[111] using the R-matrix method.

The PECs of A $^2\Delta$, X $^2\Pi$, C $^2\Sigma^+$, D $^2\Sigma^+$, B $^2\Sigma^-$, c $^4\Sigma^-$, a $^4\Sigma^-$, and d $^6\Sigma^-$ states are in excellent agreement with previous calculations[107–111] except for the X $^2\Pi$, B $^2\Sigma^-$, C $^2\Sigma^+$, and A $^2\Delta$ states in short-range regions obtained by Billoux *et al.*[108] using the RKR inversion method, which uses the extrapolation of analytical functions in the short-range and long-range regions, leading to uncertainty in their results. There are notable differences between our PECs of the E $^2\Pi$ and b $^4\Pi$ states and those computed by Kalemos *et al.*[109] as shown in panel (a) of Figs. 2 and 3, which may result from the different basis sets adopted. Compared with the cc-pVQZ basis set and cc-pV6Z basis set, the aug-cc-pwCV5Z-DK basis set and aug-cc-pV5Z basis set are augmented with diffuse functions. The aug-cc-pwCV5Z-DK basis set is also optimized with respect to the core-valence correlation energy and a small weight of core-core correlation energy and describe scalar relativistic effects using the spin-free, one-electron Douglas–Kroll–Hess (DKH) Hamiltonian. Overall, our *ab initio* PECs of CH are reliable.

The obtained PECs of CH were extrapolated using Eqs. (1) and (2) to calculate the transport collision integrals of C(^{5}S)–H(^{2}S), C(^{1}S)–H(^{2}S), C(^{1}D)–H(^{2}S), and C(^{3}P)–H(^{2}S) interactions over the temperature range of 500–50 000 K. The obtained transport collision integrals of C(^{5}S)–H(^{2}S), C(^{1}S)–H(^{2}S), and C(^{1}D)–H(^{2}S) interactions are shown in Fig. 6, and all transport collision integrals decrease with increasing temperature over the whole temperature range considered here. As shown in panel ⓒ of Fig. 6, transport collision integrals of C(^{1}S)–H(^{2}S) interaction exhibit sharp variations before about 5000 K, then change slowly, and all those lines are more concentrated, which is probably because the C(^{1}S)–H(^{2}S) dissociation limit only has one electronic state. Detailed data on the transport collision integrals over the temperature range of 500–50 000 K are given in the supplementary material. The resulting transport collision integrals were fitted to simple functional forms in the Appendix for ease of use in plasma modeling,

$$f_{\sigma^2\Omega^{(l,s)*}}(T) = A_1 + B_1 T + C_1 T^2 + D T^3 + E T^4 + F/T + G/T^2, \tag{8}$$

where A_1, B_1, C_1, D, E, F, and G are fitting parameters.

Assuming the C and H atoms in a mixture of plasma are in thermodynamic equilibrium and their numbers in ground and excited states satisfies the Boltzmann distribution equation. Carbon atoms in ground and excited states as a proportion of the total number of carbon atoms can be estimated at a temperature of T,

$$n_i = n_T \frac{g_i}{Z(T)} e^{-E_i/k_B T}, \tag{9}$$

where n_i is the number density of ith atomic excited state, g_i is the degeneracy of ith atomic excited state, E_i is the energy of ith atomic excited state, n_T is the total number density of atomic carbon, and $Z(T)$ is the electronic partition function of atomic carbon. Figure 7 shows the proportion of the ground and excited C atoms relative to

the total number of carbon atoms. At 50 000 K, the number of carbon atoms in the first excited state constitutes 15% of the total carbon atoms ($n_1 = 0.15 n_T$) and the number of carbon atoms in the second excited state is the 5% of the total carbon atoms ($n_2 = 0.05 n_T$). Moreover, the number of carbon atoms in the third excited state accounts for 20% of the total carbon atoms ($n_3 = 0.20 n_T$). Given the considered temperature range, the excitation of hydrogen atoms can be ignored. Based on the predicted numbers of C in ground and excited states, the percentages of each order of transport collision integrals for C(^{3}P)–H(^{2}S), C(^{1}D)–H(^{2}S), C(^{1}S)–H(^{2}S), and C(^{5}S)–H(^{2}S) interactions at several temperatures are then computed and presented in Table III. As shown in Table III, for the transport collision integrals of the same order, the sum of the percentages of them for the four interactions at the same temperature is considered as 100%. For example, the percentages of the contributions of transport collision integrals $\sigma^2\Omega^{(1)*}$ for C(^{3}P)–H(^{2}S), C(^{1}D)–H(^{2}S), C(^{1}S)–H(^{2}S), and C(^{5}S)–H(^{2}S) interactions at 50 000 K are 61.04%, 11.90%, 3.36%, and 23.70%, respectively, whose sum is 100%. The percentages of all orders of the transport collision integrals considered in this work for the C(^{3}P)–H(^{2}S) interaction decrease with increasing temperature. For example, the percentage of transport collision integrals $\sigma^2\Omega^{(1)*}$ for C(^{3}P)–H(^{2}S) interaction drops from 100% at 500 K to 61.04% at 50 000 K. The percentages of all orders of the transport collision integrals considered in this work for C(^{1}D)–H(^{2}S), C(^{1}S)–H(^{2}S), and C(^{5}S)–H(^{2}S) interactions increase with increasing temperature. For example, the percentage of transport collision integrals $\sigma^2\Omega^{(2,3)*}$ for the C(^{5}S)–H(^{2}S) interaction increases from 0% at 500 K to 25.28% at 50 000 K. Therefore, transport collision integrals of the interactions between the atomic ground and excited states should not be ignored in plasma modeling at high temperatures.

IV. CONCLUSIONS

In this work, we have carried out a comprehensive theoretical investigation of the transport collision integrals for the C(^{5}S)–H(^{2}S), C(^{1}S)–H(^{2}S), C(^{1}D)–H(^{2}S), and C(^{3}P)–H(^{2}S) interactions
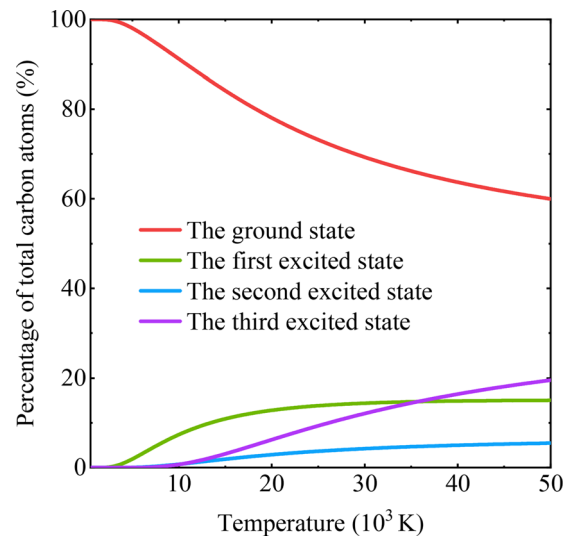

FIG. 7. Carbon atoms in ground and excited states as a percentage of the total number of carbon atoms.

TABLE III. The percentages of each order of transport collision integrals (in unit of %) for C(^{3}P)–H(^{2}S), C(^{1}D)–H(^{2}S), C(^{1}S)–H(^{2}S), and C(^{5}S)–H(^{2}S) interactions at several temperatures assuming the C and H atoms in a mixture of plasma are in thermodynamic equilibrium.

T (K)	$\sigma^2\Omega^{(1,1)*}$	$\sigma^2\Omega^{(1,2)*}$	$\sigma^2\Omega^{(1,3)*}$	$\sigma^2\Omega^{(1,4)*}$	$\sigma^2\Omega^{(2,2)*}$	$\sigma^2\Omega^{(2,3)*}$	$\sigma^2\Omega^{(2,4)*}$	$\sigma^2\Omega^{(3,3)*}$
				C(^{3}P)–H(^{2}S)				
500	100	100	100	100	100	100	100	100
5000	98.60	98.61	98.63	98.63	98.49	98.50	98.53	98.56
10 000	93.72	93.75	93.70	93.59	93.43	93.58	93.67	93.55
20 000	82.53	81.76	80.83	79.99	82.36	81.97	81.37	81.88
30 000	72.96	71.32	69.99	69.12	72.70	71.52	70.42	71.72
40 000	65.99	64.07	62.91	62.32	65.51	64.07	63.03	64.43
50 000	61.04	59.22	58.33	58.01	60.37	59.03	58.24	59.42
				C(^{1}D)–H(^{2}S)				
500	0.00	0.00	0.00	0.00	0.00	0.00	0.00	0.00
5000	1.37	1.36	1.35	1.35	1.48	1.47	1.45	1.41
10 000	5.31	5.29	5.30	5.34	5.55	5.43	5.34	5.44
20 000	9.59	9.70	9.92	10.20	9.58	9.53	9.60	9.64
30 000	11.05	11.31	11.67	12.02	10.88	11.00	11.23	11.08
40 000	11.63	11.99	12.40	12.78	11.40	11.64	11.95	11.67
50 000	11.90	12.34	12.78	13.14	11.66	11.99	12.35	11.99
				C(^{1}S)–H(^{2}S)				
500	0.00	0.00	0.00	0.00	0.00	0.00	0.00	0.00
5000	0.02	0.02	0.01	0.01	0.02	0.02	0.02	0.02
10 000	0.30	0.29	0.30	0.33	0.30	0.29	0.29	0.30
20 000	1.28	1.45	1.65	1.84	1.24	1.34	1.48	1.37
30 000	2.17	2.53	2.87	3.13	2.10	2.36	2.61	2.35
40 000	2.85	3.33	3.70	3.97	2.78	3.13	3.44	3.10
50 000	3.36	3.90	4.28	4.54	3.30	3.70	4.02	3.65
				C(^{5}S)–H(^{2}S)				
500	0.00	0.00	0.00	0.00	0.00	0.00	0.00	0.00
5000	0.01	0.01	0.01	0.01	0.01	0.01	0.01	0.01
10 000	0.67	0.67	0.70	0.74	0.72	0.70	0.70	0.71
20 000	6.59	7.09	7.60	7.97	6.82	7.16	7.55	7.11
30 000	13.82	14.84	15.47	15.73	14.32	15.12	15.74	14.85
40 000	19.53	20.61	20.99	20.93	20.31	21.16	21.58	20.80
50 000	23.70	24.54	24.61	24.31	24.67	25.28	25.39	24.94

based on the extrapolated *ab initio* PECs of ten electronic states over the temperature range of 500–50 000 K. We obtained the PECs of CH using the icMRCI+Q method with the aug-cc-pwCV5Z-DK basis set for the C atom and aug-cc-pV5Z basis set for the H atom, which were also compared with those computed by other researchers to verify the reliability of our *ab initio* data. The interactions between the excited C(^{5}S), C(^{1}S), and C(^{1}D) atoms and the ground H(^{2}S) atoms were considered for the first time. The resulting transport collision integrals were also fitted to simple functional forms for convenience in plasma modeling applications. Moreover, the results indicate that only considering the transport collision integrals for the C(^{3}P)–H(^{2}S) interaction is insufficient because the interactions between the atomic ground and excited states cannot be ignored at high temperatures. Overall, our PECs of CH are reliable. The resulting transport collision integrals are of importance for computing transport properties of high-temperature plasmas involving C and H atoms and will be also of significant interest in plasma physics and astrophysics.

SUPPLEMENTARY MATERIAL

See the supplementary material for details of transport collision integrals.

ACKNOWLEDGMENTS

23 August 2023 07:35:21

scientific calculations in this paper have been done on the HPC Cloud Platform of Shandong University.

AUTHOR DECLARATIONS
Conflict of Interest

The authors have no conflicts to disclose.

Author Contributions

Zhenlu Hou: Formal analysis (equal); Investigation (equal); Methodology (equal); Software (equal); Writing – original draft (equal). **Zhi Qin:** Conceptualization (equal); Methodology (equal); Supervision (equal); Writing – review & editing (equal). **Linhua Liu:** Funding acquisition (equal); Supervision (equal); Writing – review & editing (equal).

DATA AVAILABILITY

The data that support the findings of this study are available within the article and its supplementary material.

APPENDIX: THE FITTING PARAMETERS TO THE TRANSPORT COLLISION INTEGRALS

The fitting parameters to the transport collision integrals in Eq. (8) for the $C(^3P)$–$H(^2S)$, $C(^1D)$–$H(^2S)$, $C(^1S)$–$H(^2S)$, and $C(^5S)$–$H(^2S)$ interactions over the temperature range of 500–50 000 K are shown in Tables IV, V, VI, and VII, respectively. All the fitted functional forms deviate from the calculated data by less than 5%. The temperature ranges in which the fitting errors of the transport collision integrals for the $C(^3P)$–$H(^2S)$, $C(^1D)$–$H(^2S)$, $C(^1S)$–$H(^2S)$, and $C(^5S)$–$H(^2S)$ interactions are less than 1% are shown in Table VIII.

TABLE IV. The fitting parameters to the transport collision integrals for the $C(^3P)$–$H(^2S)$ interaction.

	A_1 (Å^2)	B_1 (10^{-4} Å^2/K)	C_1 (10^{-9} Å^2/K^2)	D (10^{-16} Å^2/K^3)	E (10^{-19} Å^2/K^4)	F (Å^2 K)	G (Å^2 K^2)
$f_{\sigma^2\Omega^{(1,1)*}}(T)$	5.6557	−3.770 65	13.0892	−2244.22	14.9325	2315.64	−192 619
$f_{\sigma^2\Omega^{(1,2)*}}(T)$	5.495 98	−4.690 61	19.0848	−3627.6	25.8591	1797.35	−175 230
$f_{\sigma^2\Omega^{(1,3)*}}(T)$	5.3267	−5.455 63	24.9795	−5129.62	38.5394	1573.89	−172 864
$f_{\sigma^2\Omega^{(1,4)*}}(T)$	5.071 96	−5.918 21	29.3654	−6343.95	49.2974	1592.92	−224 183
$f_{\sigma^2\Omega^{(2,2)*}}(T)$	5.1929	−2.049 49	3.062 56	−2.146 98	−2.509 25	3163.9	−389 500
$f_{\sigma^2\Omega^{(2,3)*}}(T)$	5.087 05	−2.431 73	4.252 05	−44.2275	−3.580 31	2608.2	−318 794
$f_{\sigma^2\Omega^{(2,4)*}}(T)$	5.1435	−3.126 64	8.079 06	−817.979	1.841 12	2057.02	−200 683
$f_{\sigma^2\Omega^{(3,3)*}}(T)$	5.620 35	−4.469 38	18.3305	−3596.31	26.5335	2300.53	−287 826

TABLE V. The fitting parameters to the transport collision integrals for the $C(^1D)$–$H(^2S)$ interaction.

	A_1 (Å^2)	B_1 (10^{-4} Å^2/K)	C_1 (10^{-9} Å^2/K^2)	D (10^{-14} Å^2/K^3)	E (10^{-19} Å^2/K^4)	F (Å^2 K)	G (Å^2 K^2)
$f_{\sigma^2\Omega^{(1,1)*}}(T)$	3.772 65	−2.414 49	7.986 43	−12.7955	7.903 74	2237.61	96 272
$f_{\sigma^2\Omega^{(1,2)*}}(T)$	3.831 18	−3.322 88	13.8733	−26.7245	19.1694	1382.3	2717.2
$f_{\sigma^2\Omega^{(1,3)*}}(T)$	3.788 74	−3.994 24	18.9969	−39.9724	30.5075	1052.98	50 519.3
$f_{\sigma^2\Omega^{(1,4)*}}(T)$	3.625 36	−4.346 52	22.3806	−49.5244	39.0945	1031.07	−26 851.4
$f_{\sigma^2\Omega^{(2,2)*}}(T)$	3.905 17	−1.544 22	1.441 77	3.888 49	−6.223 33	2519.63	124 282.2
$f_{\sigma^2\Omega^{(2,3)*}}(T)$	4.115 23	−2.434 48	6.391 03	−6.651 09	1.635 52	1595.66	172 720
$f_{\sigma^2\Omega^{(2,4)*}}(T)$	4.329 57	−3.385 55	12.4774	−21.1096	13.364	942.655	242 033
$f_{\sigma^2\Omega^{(3,3)*}}(T)$	3.999 16	−3.106 66	12.293	−23.0519	16.3143	1739.39	66 340.2

TABLE VI. The fitting parameters to the transport collision integrals for the $C(^1S)$–$H(^2S)$ interaction.

	A_1 (Å^2)	B_1 (10^{-4} Å^2/K)	C_1 (10^{-9} Å^2/K^2)	D (10^{-14} Å^2/K^3)	E (10^{-19} Å^2/K^4)	F (Å^2 K)	G (10^6 Å^2 K^2)
$f_{\sigma^2\Omega^{(1,1)*}}(T)$	2.299 01	−2.936 03	16.9587	−40.3982	33.4956	5050.38	−1.090 35
$f_{\sigma^2\Omega^{(1,2)*}}(T)$	1.061 79	−1.325 93	8.429 41	−21.2192	18.1884	5339.44	−1.212 44
$f_{\sigma^2\Omega^{(1,3)*}}(T)$	0.270 891	−0.088 816 2	1.210 29	−4.0601	4.004 27	5318.47	−1.192 21
$f_{\sigma^2\Omega^{(1,4)*}}(T)$	−0.163 861	0.685 235	−3.615 54	7.835 86	−6.055 61	5018	−1.071 89
$f_{\sigma^2\Omega^{(2,2)*}}(T)$	3.525 31	−4.611 45	26.3998	−62.4165	51.4752	4455.59	−0.968 647
$f_{\sigma^2\Omega^{(2,3)*}}(T)$	2.403 27	−3.306 43	20.0741	−49.102	41.363	5067.29	−1.205
$f_{\sigma^2\Omega^{(2,4)*}}(T)$	1.401 63	−1.875 58	12.1616	−30.8938	26.6267	5649.45	−1.401 58
$f_{\sigma^2\Omega^{(3,3)*}}(T)$	1.723 04	−2.158 84	12.8918	−31.2946	26.2382	5250.5	−1.171 48

TABLE VII. The fitting parameters to the transport collision integrals for the C(^{5}S)–H(^{2}S) interaction.

	A_1 (Å^2)	B_1 (10^{-4} Å^2/K)	C_1 (10^{-8} Å^2/K^2)	D (10^{-13} Å^2/K^3)	E (10^{-18} Å^2/K^4)	F (Å^2 K)	G (Å^2 K^2)
$f_{\sigma^2\Omega^{(1,1)*}}(T)$	6.139 14	−5.573 31	2.648 05	−5.714 23	4.472 57	2578.68	−548 647
$f_{\sigma^2\Omega^{(1,2)*}}(T)$	5.244 54	−5.397 98	2.737 89	−6.134 69	4.916 92	3037.69	−716 089
$f_{\sigma^2\Omega^{(1,3)*}}(T)$	4.354 01	−4.759 57	2.498 78	−5.720 52	4.6514	3620.46	−909 478
$f_{\sigma^2\Omega^{(1,4)*}}(T)$	3.522 69	−3.911 79	2.080 58	−4.810 63	3.940 68	4186.42	−1 086 100
$f_{\sigma^2\Omega^{(2,2)*}}(T)$	7.221 77	−5.703 47	2.503 07	−5.144 39	3.897 18	2188.11	−355 456
$f_{\sigma^2\Omega^{(2,3)*}}(T)$	6.842 56	−6.213 22	2.954 81	−6.378 86	4.990 27	2158.13	−373 145
$f_{\sigma^2\Omega^{(2,4)*}}(T)$	6.377 78	−6.331 44	3.165 66	−7.048 02	5.628 07	2367.05	−466 797
$f_{\sigma^2\Omega^{(3,3)*}}(T)$	5.747 88	−5.3057	2.575 66	−5.646 57	4.4681	3202.35	−734 212

TABLE VIII. The temperature ranges (in unit of K) in which the fitting errors of the transport collision integrals are less than 1%.

	C(^{3}P)–H(^{2}S)	C(^{1}D)–H(^{2}S)	C(^{1}S)–H(^{2}S)	C(^{5}S)–H(^{2}S)
$f_{\sigma^2\Omega^{(1,1)*}}(T)$	500–40 000	500–50 000	500–3000	500–9500
$f_{\sigma^2\Omega^{(1,2)*}}(T)$	500–10 000	1300–10 000	500–2000	500–3500
$f_{\sigma^2\Omega^{(1,3)*}}(T)$	500–10 000	500–6000	500–2500	8000–8500
$f_{\sigma^2\Omega^{(1,4)*}}(T)$	500–2000	500–2000	500–25 000	7500–8500
$f_{\sigma^2\Omega^{(2,2)*}}(T)$	500–50 000	500–20 000	500–7000	500–10 000
$f_{\sigma^2\Omega^{(2,3)*}}(T)$	500–10 000	500–4000	2000–2500	500–10 000
$f_{\sigma^2\Omega^{(2,4)*}}(T)$	500–4500	500–2500	7000–7500	500–4000
$f_{\sigma^2\Omega^{(3,3)*}}(T)$	500–10 000	500–10 000	2500–3500	500–4000

REFERENCES

[1] T. Masseron, B. Plez, S. Van Eck, R. Colin, I. Daoutidis, M. Godefroid, P.-F. Coheur, P. Bernath, A. Jorissen, and N. Christlieb, "CH in stellar atmospheres: An extensive linelist," Astron. Astrophys. **571**, A47 (2014).

[2] T. Heurlinger, Ph.D. thesis (University of Lund, 1918).

[3] T. Heurlinger and E. Hulthen, "Structure of the band spectra of burning hydrocarbons," Z. Wiss. Photogr. Photophys. Photochem. **18**, 241 (1919).

[4] P. Swings and L. Rosenfeld, "Considerations regarding interstellar molecules," Astrophys. J. **86**, 483 (1937).

[5] C. E. Moore and H. P. Broida, "CH in the solar spectrum," J. Res. Natl. Bur. Stand. Sect. A **63**, 19 (1959).

[6] D. L. Lambert, "The abundances of the elements in the solar photosphere. VIII. Revised abundances of carbon, nitrogen and oxygen," Mon. Not. R. Astron. Soc. **182**, 249 (1978).

[7] Y. Chmielewski, "The CH A$^2\Delta$-X$^2\Pi$ system in the solar spectrum," Astron. Astrophys. **133**, 83 (1984); available at https://adsabs.harvard.edu/full/1984A%26A...133...83C.

[8] A. Sauval and N. Grevesse, "Identification of vibration-rotation lines of CH in the stellar infrared spectrum," Astron. Express **1**, 153 (1985); available at https://ui.adsabs.harvard.edu/abs/1985AExpr...1..153S/abstract.

[9] D. L. Lambert, B. Gustafsson, K. Eriksson, and K. H. Hinkle, "The chemical composition of carbon stars. I. Carbon, nitrogen, and oxygen in 30 cool carbon stars in the galactic disk," Astrophys. J. Suppl. Ser. **62**, 373 (1986).

[10] P. Bernath, "The vibration–rotation emission spectrum of CH (X $^2\Pi$)," J. Chem. Phys. **86**, 4838 (1987).

[11] T. Weselak, "The relation between 5780 and 5797 diffuse interstellar bands, CH/CH$^+$ molecules, and atomic or molecular hydrogen," Astron. Astrophys. **625**, A55 (2019).

[12] T. Weselak, G. Galazutdinov, F. Musaev, and J. Krełowski, "The relation between CH and CN molecules and carriers of 5780 and 5797 diffuse interstellar bands," Astron. Astrophys. **484**, 381 (2008).

[13] G. Galazutdinov, A. Bondar, B.-C. Lee, R. Hakalla, W. Szajna, and J. Krełowski, "Survey of very broad diffuse interstellar bands," Astron. J. **159**, 113 (2020).

[14] C. Arpigny, "Spectra of comets and their interpretation," Annu. Rev. Astron. Astrophys. **3**, 351 (1965).

[15] W. S. Adams, "What lies between the stars," Publ. Astron. Soc. Pac. **53**, 73 (1941).

[16] D. J. Lien, "A reanalysis of the interstellar CH abundance," Astrophys. J. **284**, 578 (1984).

[17] O. E. H. Rydbeck, E. Kollberg, A. Hjalmarson, A. Sume, J. Ellder, and W. Irvine, "Radio observations of interstellar CH. I," Astrophys. J. Suppl. Ser. **31**, 333 (1976).

[18] A. Hjalmarson, A. Sume, J. Elider, O. Rydbeck, E. Moore, G. Huguenin, A. Sandqvist, P. Lindblad, and P. Lindroos, "Radio observations of interstellar CH. II," Astrophys. J. Suppl. Ser. **35**, 263 (1977).

[19] O. Rydbeck, J. Elldér, and W. Irvine, "Radio detection of interstellar CH," Nature **246**, 466 (1973).

[20] A. Danks, S. Federman, and D. Lambert, "The CH radical in diffuse interstellar clouds," Astron. Astrophys. **130**, 62 (1984); available at https://adsabs.harvard.edu/full/1984A%26A...130...62D.

[21] S. Federman and R. Willson, "Diffuse interstellar clouds associated with dark clouds," Astrophys. J. **260**, 124 (1982).

[22] J. G. Cohen, "Optical interstellar lines in dark clouds," Astrophys. J. **186**, 149 (1973).

[23] I. Crawford, "Ultra-high-resolution observations of the intrinsic line profiles of interstellar CH, CH$^+$ and CN," Mon. Not. R. Astron. Soc. **277**, 458 (1995).

[24] J. Whiteoak, F. Gardner, and B. Höglund, "The detection of CH in external galaxies," Mon. Not. R. Astron. Soc. **190**, 17P (1980).

[25] B. Sourd, J. Aubreton, M.-F. Elchinger, M. Labrot, and U. Michon, "High temperature transport coefficients in e/C/H/N/O mixtures," J. Phys. D: Appl. Phys. **39**, 1105 (2006).

[26] R. Janev and D. Reiter, "Collision processes of CH$_y$ and CH$_y^+$ hydrocarbons with plasma electrons and protons," Phys. Plasmas **9**, 4071 (2002).

[27] G. Sary, L. Gremillet, and B. Canaud, "Comprehensive Zakharov-type model for parametric instabilities in the corona of direct-drive targets," Phys. Plasmas **26**, 072118 (2019).

[28] T. Chapman, R. Berger, S. Brunner, and E. Williams, "Kinetic theory and Vlasov simulation of nonlinear ion-acoustic waves in multi-ion species plasmas," Phys. Rev. Lett. **110**, 195004 (2013).

[29] E. Williams, R. Berger, R. Drake, A. Rubenchik, B. Bauer, D. Meyerhofer, A. Gaeris, and T. Johnston, "The frequency and damping of ion acoustic waves in hydrocarbon (CH) and two-ion-species plasmas," Phys. Plasmas **2**, 129 (1995).

[30] Y. Kitagawa, R. Kodama, K. Takahashi, M. Mori, M. Iwata, S. Tuji, K. Suzuki, K. Sawai, K. Hamada, and K. Tanaka, "30-TW laser–plasma interactions at ILE, Osaka," Fusion Eng. Des. **44**, 261 (1999).

[31] D. Froula, D. Michel, I. Igumenshchev, S. Hu, B. Yaakobi, J. Myatt, D. Edgell, R. Follett, V. Y. Glebov, and V. Goncharov, "Laser–plasma interactions in direct-drive ignition plasmas," Plasma Phys. Controlled Fusion **54**, 124016 (2012).

[32] V. Rat, P. André, J. Aubreton, M.-F. Elchinger, P. Fauchais, and A. Lefort, "Transport properties in a two-temperature plasma: Theory and application," Phys. Rev. E **64**, 026409 (2001).

23 August 2023 07:35:21

[33]V. Colombo, E. Ghedini, and P. Sanibondi, "Thermodynamic and transport properties in non-equilibrium argon, oxygen and nitrogen thermal plasmas," Prog. Nucl. Energy **50**, 921 (2008).

[34]J. O. Hirschfelder, C. F. Curtiss, and R. B. Bird, *Molecular Theory of Gases and Liquids* (Wiley, 1964).

[35]G. Bellas Chatzigeorgis, J. B. Haskins, and J. B. Scoggins, "Transport properties for neutral C, H, N, O, and Si-containing species and mixtures from the Gordon and McBride thermodynamic database," Phys. Fluids **34**, 087106 (2022).

[36]A. Bellemans, J. B. Scoggins, R. Jaffe, and T. E. Magin, "Transport properties of carbon-phenolic gas mixtures," Phys. Fluids **31**, 096102 (2019).

[37]J. R. Stallcop, H. Partridge, and E. Levin, "Resonance charge transfer, transport cross sections, and collision integrals for $N^+(^3P)$-N $(^4S^0)$ and $O^+(^4S^0)$-O (^3P) interactions," J. Chem. Phys. **95**, 6429 (1991).

[38]Z. Ding, Z. Qin, and L. Liu, "Collision integrals for $N(^4S)$-$N(^4S)$, $N(^4S)$-$N(^2D)$ and $N(^4S)$-$N(^2P)$ interactions," Phys. Fluids **35**, 027127 (2023).

[39]E. Levin, H. Partridge, and J. R. Stallcop, "Collision integrals and high temperature transport properties for NN, OO, and NO," J. Thermophys. Heat Transfer **4**, 469 (1990).

[40]M. Buchowiecki and P. Szabó, "N-H collision integrals with study of repulsive interactions," Plasma Sources Sci. Technol. **31**, 045010 (2022).

[41]M. J. Wright, H. H. Hwang, and D. W. Schwenke, "Recommended collision integrals for transport property computations. II. Mars and venus entries," AIAA J. **45**, 281 (2007).

[42]A. Murphy, "Transport coefficients of hydrogen and argon–hydrogen plasmas," Plasma Chem. Plasma Process. **20**, 279 (2000).

[43]H. Partridge, J. R. Stallcop, and E. Levin, "Transport cross sections and collision integrals for $N(^4S^o)$-$O^+(^4S^o)$ and $N^+(^3P)$-$O(^3P)$ interactions," Chem. Phys. Lett. **184**, 505 (1991).

[44]J. R. Stallcop, H. Partridge, and E. Levin, "Collision integrals for the interaction of the ions of nitrogen and oxygen in a plasma at high temperatures and pressures," Phys. Fluids B **4**, 386 (1992).

[45]M. Buchowiecki and P. Szabó, "Collision integrals for nitrogen and hydrogen ionized gas: The exact values and assessment of approximations," Plasma Chem. Plasma Process. **43**, 449 (2023).

[46]L. S. Tee, S. Gotoh, and W. E. Stewart, "Molecular parameters for normal fluids. Lennard-Jones 12–6 Potential," Ind. Eng. Chem. Fundam. **5**, 356 (1966).

[47]X. Wang, S. Ramírez-Hinestrosa, J. Dobnikar, and D. Frenkel, "The Lennard-Jones potential: When (not) to use it," Phys. Chem. Chem. Phys. **22**, 10624 (2020).

[48]R. Zhou, Z. Qiu, C. Sun, and B. Bai, "Entrance loss of capillary flow in narrow slit nanochannels," Phys. Fluids **35**, 042005 (2023).

[49]S. Kazem Manzoorolajdad, H. Hamzehpour, and J. Sarabadani, "Electro-osmotic flow in different phosphorus nanochannels," Phys. Fluids **35**, 042006 (2023).

[50]B. Shan, L. Ju, W. Su, Z. Guo, and Y. Zhang, "Non-equilibrium flow of van der Waals fluids in nano-channels," Phys. Fluids **35**, 052004 (2023).

[51]D. Salem, "Collision integrals and viscosity coefficients of argon–carbon thermal plasmas: Comparison using different interaction potentials," Phys. Fluids **34**, 126602 (2022).

[52]M. Buchowiecki, "High-temperature collision integrals for m-6-8 and Hulburt-Hirschfelder potentials," Int. J. Thermophys. **43**, 38 (2022).

[53]M. Klein and H. Hanley, "m-6-8 potential function," J. Chem. Phys. **53**, 4722 (1970).

[54]H. M. Hulburt and J. O. Hirschfelder, "Potential energy functions for diatomic molecules," J. Chem. Phys. **9**, 61 (1941).

[55]J. C. Rainwater, P. M. Holland, and L. Biolsi, "Binary collision dynamics and numerical evaluation of dilute gas transport properties for potentials with multiple extrema," J. Chem. Phys. **77**, 434 (1982).

[56]Y. Liu, F. Shakib, and M. Vinokur, "A comparison of internal energy calculation methods for diatomic molecules," Phys. Fluids A **2**, 1884 (1990).

[57]J. G. Kim and G. Park, "Thermochemical nonequilibrium parameter modification of oxygen for a two-temperature model," Phys. Fluids **30**, 016101 (2018).

[58]T.-C. Lim, "Application of extended-Rydberg parameters in general Morse potential functions," J. Math. Chem. **49**, 1086 (2011).

[59]P. Kuntz and A. Roach, "Ion-molecule reactions of the rare gases with hydrogen. I. Diatomics-in-molecules potential energy surface for ArH_2^+," J. Chem. Soc., Faraday Trans. 2 **68**, 259 (1972).

[60]F. Sharipov, "Direct simulation Monte Carlo method based on ab initio potential: Recovery of transport coefficients of multi-component mixtures of noble gases," Phys. Fluids **34**, 097114 (2022).

[61]P. Valentini, M. S. Grover, N. Bisek, and A. Verhoff, "Molecular simulation of flows in thermochemical non-equilibrium around a cylinder using ab initio potential energy surfaces for N_2 + N and N_2 + N_2 interactions," Phys. Fluids **33**, 096108 (2021).

[62]M. S. Grover and P. Valentini, "Ab initio simulation of hypersonic flows past a cylinder based on accurate potential energy surfaces," Phys. Fluids **33**, 051704 (2021).

[63]V. Yurkiv, J. Wu, S. Halder, R. Granda, A. Sankaran, A. L. Yarin, and F. Mashayek, "Water interaction with dielectric surface: A combined ab initio modeling and experimental study," Phys. Fluids **33**, 042012 (2021).

[64]R. A. Aziz, A. R. Janzen, and M. R. Moldover, "Ab initio calculations for helium: A standard for transport property measurements," Phys. Rev. Lett. **74**, 1586 (1995).

[65]M. Buchowiecki, "The elastic scattering cross sections of the N^+-H and N-H^+ collisions for the transport theory," At. Data Nucl. Data Tables **151**, 101574 (2023).

[66]J. N. Murrell, *Molecular Potential Energy Functions* (John Wiley, 1984).

[67]M. Agúndez, J. Cernicharo, L. Decin, P. Encrenaz, and D. Teyssier, "Confirmation of circumstellar phosphine," Astrophys. J. Lett. **790**, L27 (2014).

[68]G. Chen, Z. Qin, J. Li, and L. Liu, "A global CHIPR potential energy surface of PH_2 (X^2B_1) via extrapolation to the complete basis set limit and the dynamics of $P(^2D)+H_2$ $(X^1\Sigma^+_g)$ → PH $(X^3\Sigma^-)+H(^2S)$," Phys. Chem. Chem. Phys. **24**, 19371 (2022).

[69]X. Li, Z. Qin, J. Li, and L. Liu, "An accurate NH_2 (X^2A'') CHIPR potential energy surface via extrapolation to the complete basis set limit and dynamics of the $N(^2D)$ + H_2 $(X^1\Sigma^+_g)$ reaction," Phys. Chem. Chem. Phys. **24**, 26564 (2022).

[70]X. Li, Z. Qin, G. Chen, and L. Liu, "Reaction dynamics of $C(^3P)$+ Si_2 (X $^3\Sigma^-_g$) → $Si(^3P)+SiC(X$ $^3\Pi)$ on a global CHIPR potential energy surface of the ground state $Si_2C(X$ $^1A_1)$," Mon. Not. R. Astron. Soc. **522**, 3049 (2023).

[71]G. Chen, Z. Qin, X. Li, and L. Liu, "Reaction dynamics of $P(^4S)$+ $O_2(X^3\Sigma^-)$ → $O(^3P)$+ $PO(X^2\Pi)$ on a global CHIPR potential energy surface of PO_2 (X $^2A_1$): implication for atmospheric modelling," Atmos. Chem. Phys. (published online 2023).

[72]A. Varandas, "Combined-hyperbolic-inverse-power-representation of potential energy surfaces: A preliminary assessment for H_3 and HO_2," J. Chem. Phys. **138**, 054120 (2013).

[73]A. Varandas, "Accurate combined-hyperbolic-inverse-power-representation of ab initio potential energy surface for the hydroperoxyl radical and dynamics study of O+OH reaction," J. Chem. Phys. **138**, 134117 (2013).

[74]C. M. Rocha and A. J. Varandas, "A general code for fitting global potential energy surfaces via CHIPR method: Direct-fit diatomic and tetratomic molecules," Comput. Phys. Commun. **258**, 107556 (2021).

[75]C. M. Rocha and A. J. Varandas, "A general code for fitting global potential energy surfaces via CHIPR method: Triatomic molecules," Comput. Phys. Commun. **247**, 106913 (2020).

[76]C. Rocha and A. Varandas, "Accurate CHIPR potential energy surface for the lowest triplet state of C_3," J. Phys. Chem. A **123**, 8154 (2019).

[77]A. Sanon and J. Baronnet, "Transport coefficients of Ar/C/H/O/N systems thermal plasma at atmospheric pressure," IOP Conf. Ser.: Mater. Sci. Eng. **29**, 012003 (2012).

[78]H. Werner, P. Knowles, G. Knizia, F. Manby, M. Schütz, P. Celani, W. Györffy, D. Kats, T. Korona, and R. Lindh, see http://www.molpro.net for MOLPRO, a package of ab initio programs, version 2015.1.

[79]H.-J. Werner, P. J. Knowles, F. R. Manby, J. A. Black, K. Doll, A. Heßelmann, D. Kats, A. Köhn, T. Korona, and D. A. Kreplin, "The Molpro quantum chemistry package," J. Chem. Phys. **152**, 144107 (2020).

[80]H. J. Werner and P. J. Knowles, "A second order multiconfiguration SCF procedure with optimum convergence," J. Chem. Phys. **82**, 5053 (1985).

23 August 2023 07:35:21

[81]P. J. Knowles and H.-J. Werner, "An efficient second-order MC SCF method for long configuration expansions," Chem. Phys. Lett. **115**, 259 (1985).

[82]H. J. Werner and P. J. Knowles, "An efficient internally contracted multiconfiguration–reference configuration interaction method," J. Chem. Phys. **89**, 5803 (1988).

[83]P. J. Knowles and H.-J. Werner, "An efficient method for the evaluation of coupling coefficients in configuration interaction calculations," Chem. Phys. Lett. **145**, 514 (1988).

[84]P. J. Knowles and H.-J. Werner, "Internally contracted multiconfiguration-reference configuration interaction calculations for excited states," Theor. Chim. Acta **84**, 95 (1992).

[85]K. Shamasundar, G. Knizia, and H.-J. Werner, "A new internally contracted multi-reference configuration interaction method," J. Chem. Phys. **135**, 054101 (2011).

[86]Z. Qin, T. Bai, and L. Liu, "An ab initio study for the photodissociation of HCl and HF," Mon. Not. R. Astron. Soc. **516**, 550 (2022).

[87]T. Bai, Z. Qin, and L. Liu, "Radiative association for the formation of MgO," Mon. Not. R. Astron. Soc. **500**, 2496 (2021).

[88]H. Meng, Z. Qin, and L. Liu, "Formation of CO through C $(2s^2 2p^2\ ^3P)$ and O $(2s^2 2p^4\ ^3P)$ radiative association," Astrophys. J. **935**, 148 (2022).

[89]S. Zhang, Z. Qin, and L. Liu, "A quantum mechanical calculation of the CN radiative association," Mon. Not. R. Astron. Soc. **515**, 6066 (2022).

[90]Z. Hou, Z. Qin, and L. Liu, "Formation of SiO$^+$ through radiative association of Si$^+$($3s^2 3p\ ^2P_u$) and O($2s^2 2p^4\ ^3P_g$)," Astron. Astrophys. **672**, A25 (2023).

[91]N. J. DeYonker, K. A. Peterson, and A. K. Wilson, "Systematically convergent correlation consistent basis sets for molecular core—valence correlation effects: The third-row atoms gallium through krypton," J. Phys. Chem. A **111**, 11383 (2007).

[92]D. Feller, "Application of systematic sequences of wave functions to the water dimer," J. Chem. Phys. **96**, 6104 (1992).

[93]D. Feller, "The use of systematic sequences of wave functions for estimating the complete basis set, full configuration interaction limit in water," J. Chem. Phys. **98**, 7059 (1993).

[94]A. A. Petersson, A. Bennett, T. G. Tensfeldt, M. A. Al-Laham, W. A. Shirley, and J. Mantzaris, "A complete basis set model chemistry. I. The total energies of closed-shell atoms and hydrides of the first-row elements," J. Chem. Phys. **89**, 2193 (1988).

[95]G. Petersson and M. A. Al-Laham, "A complete basis set model chemistry. II. Open-shell systems and the total energies of the first-row atoms," J. Chem. Phys. **94**, 6081 (1991).

[96]A. Dalgarno and W. Davison, "The calculation of van der Waals interactions," Adv. At. Mol. Phys. **2**, 1 (1966).

[97]Z.-C. Yan, J. F. Babb, A. Dalgarno, and G. Drake, "Variational calculations of dispersion coefficients for interactions among H, He, and Li atoms," Phys. Rev. A **54**, 2824 (1996).

[98]P.-G. Yan, "Precision calculations of long-range interactions among three atomic systems," Ph.D. thesis (University of New Brunswick, 2018).

[99]M. Semenov, N. El-Kork, S. N. Yurchenko, and J. Tennyson, "Rovibronic spectroscopy of PN from first principles," Phys. Chem. Chem. Phys. **23**, 22057 (2021).

[100]Z. Qin, T. Bai, and L. Liu, "Temperature-dependent direct photodissociation cross sections and rates of AlCl," Mon. Not. R. Astron. Soc. **508**, 2848 (2021).

[101]H. Friedrich and H. Friedrich, *Theoretical Atomic Physics* (Springer, Berlin, 2006).

[102]A. Laricchiuta, G. Colonna, D. Bruno, R. Celiberto, C. Gorse, F. Pirani, and M. Capitelli, "Classical transport collision integrals for a Lennard-Jones like phenomenological model potential," Chem. Phys. Lett. **445**, 133 (2007).

[103]G. Palmer and M. Wright, "A comparison of methods to compute high-temperature gas thermal conductivity," AIAA Paper No. 2003-3913, 2003, p. 3913.

[104]D. D. Konowalow, J. O. Hirschfelder, and B. Linder, "Low-temperature, low-pressure transport coefficients for gaseous oxygen and sulfur atoms," J. Chem. Phys. **31**, 1575 (1959).

[105]H. Knof, E. Mason, and J. Vanderslice, "Interaction energies, charge exchange cross sections, and diffusion cross sections for N$^+$-N and O$^+$-O collisions," J. Chem. Phys. **40**, 3548 (1964).

[106]M. Capitelli, C. Guidotti, and U. Lamanna, "Potential energy curves and excitation transfer cross sections of excited hydrogen atoms," J. Phys. B: At. Mol. Phys. **7**, 1683 (1974).

[107]D. B. Abdallah, F. Najar, N. Jaidane, Z. B. Lakhdar, and P. Honvault, "Ab initio potential energy surfaces for the study of rotationally inelastic CH (X$^2\Pi$)+ H (^{2}S) collisions," Chem. Phys. Lett. **456**, 7 (2008).

[108]T. Billoux, Y. Cressault, and A. Gleizes, "Tables of radiative transition probabilities for the main diatomic molecular systems of OH, CH, CH$^+$, CO and CO$^+$ occurring in CO-H$_2$ syngas-type plasma," J. Quant. Spectrosc. Radiat. Transfer **133**, 434 (2014).

[109]A. Kalemos, A. Mavridis, and A. Metropoulos, "An accurate description of the ground and excited states of CH," J. Chem. Phys. **111**, 9536 (1999).

[110]C. Song, H. Han, Y. Zhang, Y. Yu, and T. Gao, "Potential-energy curves of the CH radical molecule under spin-orbit coupling," Can. J. Phys. **86**, 1145 (2008).

[111]K. Chakrabarti, R. Ghosh, and B. Choudhury, "R-matrix calculation of bound and continuum states of CH," J. Phys. B: At. Mol. Opt. Phys. **52**, 105205 (2019).

23 August 2023 07:35:21